Improvement of mechanical toughness of poly(lactic acid) by addition of ethylene-vinyl acetate copolymer

Daisuke Kugimoto,[1)] Shingo Kouda,[1)]

Masayuki Yamaguchi[2)*]

1) Polymer Materials Research Laboratory, Tosoh Corporation
1-8 Kasumi, Yokkaichi, Mie 510-8540 JAPAN

2) School of Materials Science,
Japan Advanced Institute of Science and Technology
1-1 Asahidai, Nomi, Ishikawa 923-1292 JAPAN

* Corresponding to Masayuki Yamaguchi
School of Materials Science, Japan Advanced Institute of Science and Technology
1-1 Asahidai, Nomi, Ishikawa 923-1292 Japan
Phone +81-761-51-1621, Fax +81-761-51-1149
E-mail: m_yama@jaist.ac.jp

Abstract

We investigated the structure and properties of binary blends comprising poly(lactic acid) (PLA) as a matrix and ethylene–vinyl acetate copolymer (EVA), by considering the effect of the vinyl acetate (VAc) content in EVA. The interfacial tension with PLA was found to decrease with increasing the VAc content. Therefore, blends comprising EVA with a high VAc content have fine EVA particles, and exhibit marked mechanical toughness and good transparency. Although pure PLA is prone to brittle fractures, the addition of EVA leads to shear yielding, which is prominent when the matrix ligament thickness is shorter than a critical value. The cavitation process in the dispersed EVA particles is also responsible for the mechanical toughness, which is obvious in EVA with a high VAc content.

Keywords: Poly(lactic acid); Mechanical properties; Polymer blends; Transparency; Morphology

Introduction

Global concern about plastic waste has accelerated the use of poly(lactic acid) (PLA), which is one of the best-known biodegradable plastics produced from renewable resources. Recently, the manufacturing cost of PLA has decreased greatly. Therefore, it is expected to become a substitute for conventional plastics such as polypropylene. PLA has several advantages such as high modulus and transparency. However, its applications remain limited because it has poor impact strength, low heat distortion temperature, and poor melt elasticity [1-4]. The heat resistance of PLA can be greatly improved by increasing its crystallinity [4-6], and several methods of enhancing its melt elasticity have been proposed recently [4,7-10].

The addition of a rubbery material is a well-known general technique for improving the mechanical toughness of most brittle plastics, although a recent study revealed that the mechanical toughness of PLA is improved by an appropriate thermal history [11,12]. The addition of rubber is known to provide energy dissipation owing to pronounced plastic deformation under stress, such as shear yielding of a matrix between rubber particles, multiple crazing starting from rubber particles, and cavitation in rubber particles [13-15]. To date, various materials have been used to improve the mechanical toughness of PLA. These include poly(ε-caprolactone) [16], poly(butylene succinate) [17,18], poly(butylene adipate–*co*-terephthalate) (PBAT) [19], thermoplastic polyurethane elastomers (TPUs) [20], and core–shell latex rubbers [21]. Han and Huang [20] reported that the addition of TPU greatly improved the mechanical toughness of PLA because it had good compatibility with PLA due to hydrogen bonding. They also

confirmed that the matrix ligament thickness plays an important role in mechanical behavior. In the case of blends with PBAT, which has been commercialized as an impact modifier for PLA [19], the mechanical toughness is further improved by the addition of a reactive modifier [22]. A similar technique has also been reported by Harada et al. [17] and Li and Shimizu [23].

Even a polymer having poor compatibility with PLA, such as linear low-density polyethylene (LLDPE), can improve mechanical toughness by controlling the phase-separated structure, as reported by Anderson et al. [24]. In general, PLA/LLDPE blends have low impact strength owing to their coarse morphology, which leads to excess stress concentration. This is reasonable because the system has a large interfacial tension. However, the addition of a block copolymers composed of PLA and polyethylene (PE) as a compatibilizer resulted in a finer morphology with strong adhesion at interface, which greatly improves the impact strength.

Poly(vinyl acetate) (PVAc) is miscible with PLA [25], whereas PE is not. Therefore, it is supposed that the compatibility/miscibility of PLA with ethylene–vinyl acetate copolymer (EVA) depends on the vinyl acetate (VAc) content in EVA. In fact, EVA with more than 50 wt.% of VAc is capable of improving the impact strength and elongation at break of PLA [26-28].

In the present study, we first evaluated the effect of the VAc content in EVA on its compatibility with PLA. Based on this information, we investigated the influence of the dispersion of EVA particles on the mechanical and optical properties of the blends.

Experimental

Materials

We used a commercially available poly(lactic acid) (PLA) with an L-lactide content of 98.5% and a melting point of 167 °C. The number- and weight-average molecular weights evaluated by size exclusion chromatography with a polystyrene standard were $M_n = 1.03 \times 10^5$ and $M_w = 1.82 \times 10^5$, respectively. We used three EVA copolymers with various vinyl acetate (VAc) contents. In the present study, the numerals in the EVA sample codes represent the VAc content as a weight fraction. EVA25 was crystalline and had a melting point (T_m) of approximately 75 °C. The other EVA samples were amorphous. The characteristics reported by the producer are summarized in Table 1, with the solubility parameter δ calculated by the group contribution method proposed by Small [29].

Table 1 Characteristics of polymers

Sample code	VAc (wt.%)	Density (kg/m^3)	δ ($MPa^{0.5}$)	Grade, Producer
PLA	−	1240	19.6	Ingeo 4032D, NatureWorks
EVA25	25	948	17.7	Ultrathene 640, Tosoh
EVA50	50	1000	17.9	Levapren 500, Lanxess
EVA80	80	1110	18.6	Levapren 800, Lanxess

Sample preparation

We dried the PLA and EVA at 80 °C for 3 h to avoid hydrolysis [6], then mixed

them in the molten state using an internal batch mixer (Labo-Plastmill; Toyo Seiki Seisaku-sho, Japan) at 180 °C for 5 min. The blade rotation speed was 120 rpm, which provided a shear rate of 114 s^{-1} between the blades and the inner wall. The blend ratios of PLA/EVA by weight were 90/10, 80/20, and 70/30. We also added the following thermal stabilizers: pentaerythritol tetrakis(3-(3,5-di-tert-butyl-4-hydroxyphenyl)propionate) (Irganox 1010; Ciba Specialty Chemicals, Switzerland); and 6-[3-(3-tert-butyl-4-hydroxy-5-methylphenyl)propoxy]-2,4,8,10-tetra-tert-butyldibenzo[d,f][1,3,2] dioxaphosphepin (Sumilizer GP; Sumitomo Chemical, Japan). The content of each stabilizer was 3000 ppm. The blend samples were compression-molded into flat sheets of various thicknesses at 200 °C, then quenched at 25 °C.

Measurements

The shear viscosities of the raw materials at 190 °C as a function of shear rate were evaluated using a capillary rheometer (Capilograph; Toyo Seiki Seisaku-sho, Japan). A circular die with 20 mm in length and 1 mm in diameter was employed. Neither Bagley nor Rabinowitsch corrections were performed.

The refractive index at 589 nm and 25 °C was measured using an Abbe refractometer (NAR-1T; Atago, Japan) with 1-bromonaphthalene as a contact liquid.

The contact angle measurements were carried out at 25 °C on the surfaces of compression-molded sheets. The contact angle θ was evaluated using a drop-shaped analysis system (DMs-401; Kyowakaimenkagaku, Japan). We used distilled water (H_2O, γ_L = 72.8 mN/m, γ_L^d = 21.8 mN/m, and γ_L^p = 51.0 mN/m) and methylene

iodide (CH_2I_2, γ_L = 50.8 mN/m, γ_L^d = 49.5 mN/m, and γ_L^p = 1.3 mN/m) as probe liquids.

The morphologies of the blends were examined by scanning electron microscopy (SEM; TM3030; Hitachi, Japan) and transmission electron microscopy (TEM; JEM-2100F; JEOL, Japan). Prior to the SEM observation, the cryogenically fractured surface of the compression-molded sheet was coated with gold. For the TEM investigation, we cut a thin sample (approximately 100 nm) from the compression-molded sheet using an ultramicrotome, and stained it with RuO_4 prior to examination. The diameters of the dispersed EVA particles were evaluated from the SEM images using image analysis software (Image J; National Institutes of Health, MD, USA).

The temperature dependence of the dynamic tensile moduli in the solid state—the tensile storage modulus E' and the loss modulus E''— at 10 Hz was determined using a dynamic mechanical analyzer (Rheogel-E4000; UBM, Japan) in the temperature range from -100 to 200 °C. The heating rate was 5 °C/min. We used rectangular samples (5 mm wide × 20 mm long × 1 mm thick).

The optical transparency was evaluated using a UV–visible analyzer (Lambda; Perkin-Elmer, MA, USA) and a haze meter (NDH-7000; Nippon Denshoku Industries, Japan) using a white light-emitting diode as a light source. Both measurements were carried out at 25 °C using a 0.1 mm-thick sheet.

The crystalline structures of the samples were investigated by wide-angle X-ray diffraction (WAXD; Smart Lab, Rigaku, Japan) using CuKα radiation at 30 mA and 40 kV. The sample sheet was 0.1 mm thick and the scan speed was 10°/min.

Tensile tests were carried out at 25 °C using a tensile testing machine (Tensilon RTE-1210; Orientec, Japan) at a crosshead speed of 200 mm/min. The samples were cut into 0.1 mm-thick dumbbell-shaped specimens (ASTM 1822L).

The impact strength was evaluated with a film impact tester (Toyo Seiki Seisaku-sho, Japan) at 25 °C using 0.1 mm-thick sheets. The measurements were performed at least five times, and the average value was calculated.

Results and Discussion

Characteristics of PVA and EVA

We evaluated the shear viscosities of the raw materials because the viscosity ratio plays a dominant role in the structure of an immiscible polymer blend [9,30]. As shown in Fig. 1, the shear viscosity of PLA was higher than those of the EVA samples over a wide range of shear rates. EVA80 had a slightly lower viscosity than the other EVA samples. Furthermore, the EVA samples exhibited marked non-Newtonian behavior compared with PLA. This was as expected because EVA has a broad relaxation time distribution owing to a broad molecular weight distribution and a long-chain branch structure. Therefore, the rheological properties are similar to those of low-density polyethylene, not linear polyethylene [31].

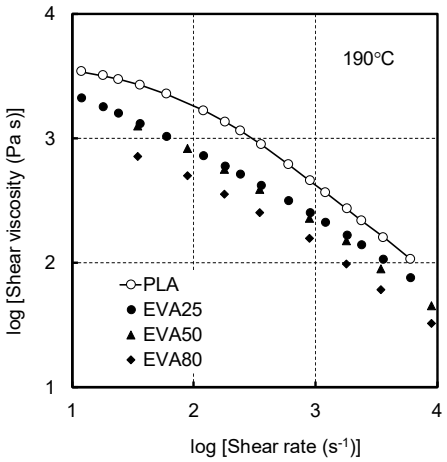

Figure 1 Apparent shear viscosity versus shear rate at 190 °C.

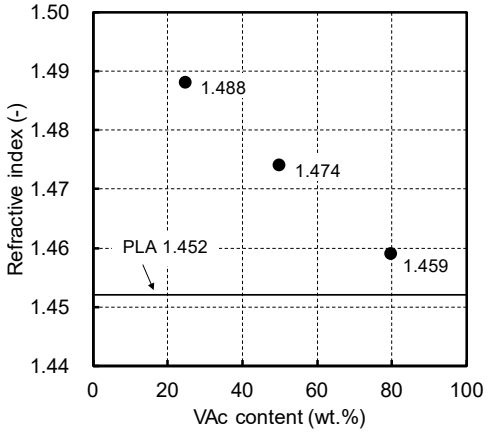

Figure 2 Refractive indices of EVA samples as a function of the VAc content. The solid line represents the refractive index of PLA.

We also determined the refractive indices of the raw materials at 25 °C to discuss the transparencies of the blends. Fig. 2 shows the refractive index at 589 nm of EVA as a function of the VAc content. As reported by Takahashi et al., the refractive index decreased as the VAc content increased [32]. The refractive index of PLA was lower than those of the EVA samples used in the present study. Therefore, it was reasonable to assume that a binary blend composed of PLA and EVA with a high VAc content would have good transparency.

We determined the surface tensions of PLA, EVA25, and EVA80 by the contact angle θ using the following equation [33] to predict the interfacial tension, which affects the blend morphology and adhesive strength between phases to a great extent [34-38]:

$$\gamma_L\left(1+\cos\theta\right)=2\sqrt{\gamma^d\gamma_L^d}+2\sqrt{\gamma^p\gamma_L^p}\ , \tag{1}$$

where γ_L is the surface tension of the probe liquids, and γ_L^d and γ_L^p are the dispersive and polar components, respectively. Furthermore, γ^d and γ^p are those of a measured polymer, and their sum is the surface tension of the polymer, that is, γ. Table 2 summarizes the contact angles and the calculated surface tensions.

Table 2 Contact angles and calculated surface tensions

Samples	Contact angle (degree)		Surface tension and its components (mN/m)		
	H_2O	CH_2I_2	γ	γ^d	γ^p
PLA	73.4	42.9	41.3	33.7	7.6
EVA25	85.1	43.7	38.1	35.5	2.7
EVA80	73.8	40.7	42.0	35.0	7.0

Furthermore, the interfacial tension $\Gamma_{PLA/EVA}$ was estimated from the surface tension and its components using the following equation [39]:

$$\Gamma_{PLA/EVA}=\gamma_{PLA}+\gamma_{EVA}-4\frac{\gamma_{PLA}^d\gamma_{EVA}^d}{\gamma_{PLA}^d+\gamma_{EVA}^d}-4\frac{\gamma_{PLA}^p\gamma_{EVA}^p}{\gamma_{PLA}^p+\gamma_{EVA}^p}\ . \tag{2}$$

Table 3 shows the calculated interfacial tension with the difference in the solubility parameters, $\Delta\delta$, predicted using the Small's method.

Table 3 Interfacial tension Γ and solubility parameter difference $\Delta\delta$

Polymer pair	$\Gamma_{PLA/EVA}$ (mN/m)	$\Delta\delta$ (MPa$^{0.5}$)
PLA/EVA25	2.4	1.9
PLA/EVA50	-	1.7
PLA/EVA80	0.05	1.0

Good compatibility was suggested between PLA and the EVA samples with a high VAc content. This was as expected because poly(vinyl acetate) is known to be miscible with PLA [25]. In the case of EVA80, in particular, the interaction parameter with PLA was markedly small. Even though the value was calculated based on the surface tension in the solid state, good compatibility with PLA in the molten state—at melt-mixing—was expected for EVA80.

Blend Morphology

SEM images of the blend samples are shown in Fig. 3. The dispersed droplets were fine, especially in the blends with EVA80, as predicted by the interfacial tension [30]. The droplet diameter increased with the EVA content because EVA particles coalesce more frequently at high concentrations. The mean droplet diameter (d) and its distribution (σ) were calculated using the following equations [40]:

$$\ln d = \frac{\sum_{i=1}^{N} n_i \ln d_i}{\sum_{i=1}^{N} n_i}, \tag{3}$$

$$\ln \sigma = \sqrt{\frac{\sum_{i=1}^{N} n_i \left(\ln d_i - \ln d\right)^2}{\sum_{i=1}^{N} n_i}}, \tag{4}$$

where n_i is the number of droplets with a diameter of d_i, and N is the total number of droplets. A large σ value indicates a broad distribution of particle sizes. When all

particles have the same diameter, i.e. monodisperse, σ is 1. The mean diameter of the droplets *d* and its distribution σ are summarized in Table 4. It should be noted that the droplet diameters of PLA/EVA50 (90/10), PLA/EVA80 (90/10), and PLA/EVA80 (80/20) were smaller than 1 μm.

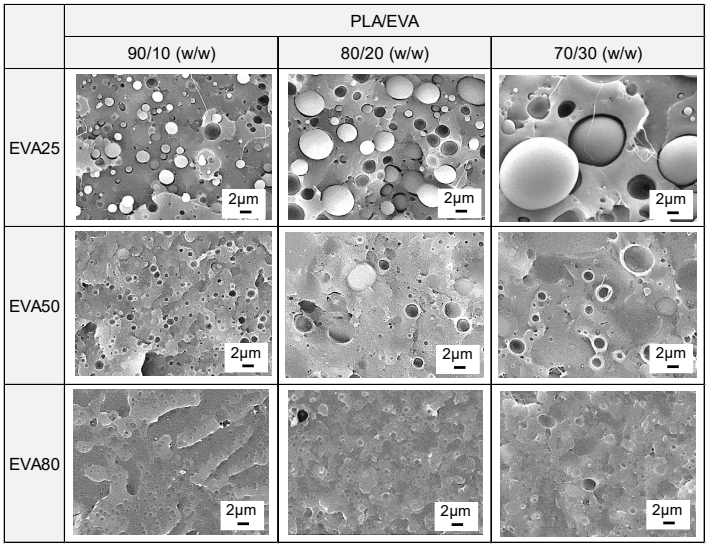

Figure 3 SEM images of fractured surfaces of the PLA/EVA blends.

Table 4 Size of dispersed droplets and matrix ligament thicknesses

Samples	PLA (wt.%)	EVA (wt.%)	ϕ (vol.%)	*d* (μm)	σ (-)	*T* (μm)
PLA/EVA25	90	10	0.127	1.4	1.80	2.05
	80	20	0.246	2.2	1.89	2.21
	70	30	0.359	4.4	2.28	7.69
PLA/EVA50	90	10	0.121	0.8	1.39	0.68
	80	20	0.237	1.4	1.92	1.73
	70	30	0.347	1.6	2.03	1.80
PLA/EVA80	90	10	0.110	0.6	1.24	0.47
	80	20	0.218	0.8	1.35	0.39
	70	30	0.324	1.1	1.61	0.60

ϕ: volume fraction of ethylene–vinyl acetate copolymer (EVA); *d*: particle diameter; σ: particle diameter distribution; *T*: matrix ligament thickness.

We calculated the matrix ligament thickness T, that is, the distance between the surface-to-surface interparticle distance, using the following equation [40]:

$$T = d\left[\left(\frac{\pi}{6\phi}\right)^{1/3} \exp\left(1.5\ \ln^2\sigma\right) - \exp\left(0.5\ \ln^2\sigma\right)\right], \quad (5)$$

where ϕ is the volume fraction of the dispersed droplets. The results are also shown in Table 4.

Fig. 4 shows the temperature dependence of the dynamic tensile moduli, that is, the storage modulus E' and the loss modulus E''. The PLA sheet obtained under such cooling conditions—quenched at 25 °C—had no crystallinity, as shown later. Therefore, E' dropped off sharply at the glass transition temperature T_g at approximately 60 °C. Beyond T_g, E' increased owing to cold crystallization; i.e., crystallization during heating. This is a well-known phenomenon for a quenched crystalline polymer with no/few crystallinity including PLA [1,4,6,12,41]. Since the molecular motion is allowed beyond the T_g, crystallization occurs, leading to the modulus increase. The E' value then decreased again at approximately 165 °C owing to the melting of the crystals. These dynamic mechanical behaviors of quenched PLA were already reported elsewhere [4,6,12]. In the case of pure EVA, E' decreased at T_g; this was more obvious in EVA50 and EVA80, i.e., the non-crystalline EVA samples. For EVA25, E' decreased gradually owing to the crystallinity, and fell off sharply at T_m, that is, 75 °C. The E'' peak of EVA25 ascribed to T_g was broad owing to its crystallinity. These dynamic mechanical properties were almost the same with the reported ones [32,42]. For EVA80, the E'' peak was located at a high temperature, suggesting a high T_g. The blends had similar

dynamic mechanical properties compared with the pure PLA—the matrix of the blends—although the E' decreased slightly at approximately the T_g of the EVA phase. Although a significantly low interfacial tension was expected between PLA and EVA80, the peak temperatures in the E'' curve, ascribed to the T_g values of both phases, were not affected, demonstrating that mutual dissolution hardly occurred.

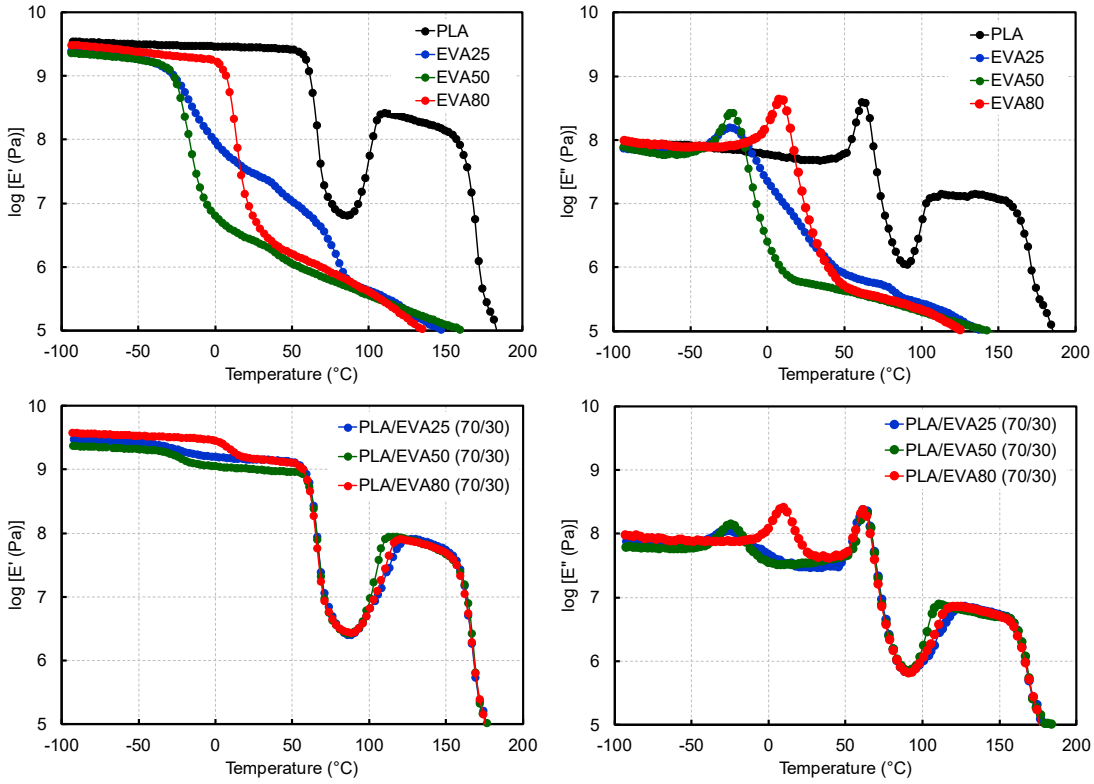

Figure 4 Temperature dependencies of tensile storage modulus E' and loss modulus E'' at 10 Hz.

Fig. 5 shows the WAXD profiles of the pure samples. For PLA, there were no diffraction peaks attributable to a crystalline structure, suggesting that the PLA sheet was non-crystalline, as corroborated by the dynamic mechanical properties shown in Fig. 4. EVA25 had a strong diffraction peak, whereas both EVA50 and EVA80 produced

only a broad amorphous peak. The blends with EVA50 and EVA80 also produced amorphous peaks (not presented here).

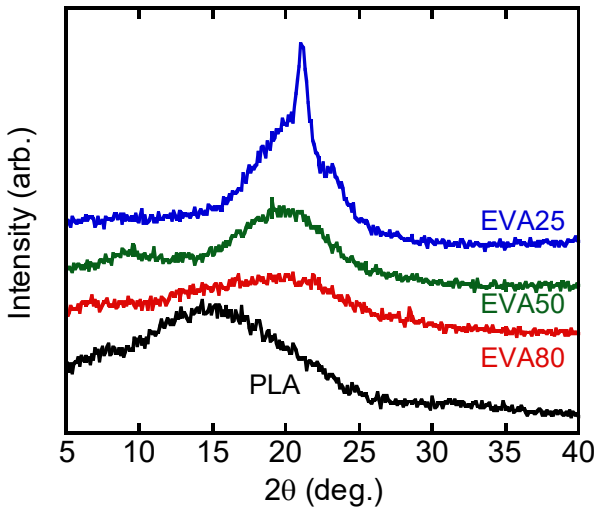

Figure 5 Wide-angle X-ray diffraction (WAXD) profiles of pure samples.

Optical transparency

Fig. 6 shows the light transmittance values, and Table 5 summarizes the haze values of the samples. We performed both measurements at 25 °C using 0.1 mm-thick sheets. The light transmittance of the blends, which corresponds with the haze values, decreased with increasing the EVA content owing to light scattering. It should be noted that the transparency depended strongly on the VAc content in EVA. Blends with EVA80 in particular exhibited good transparency because there were only small differences in the refractive indices with fine droplets.

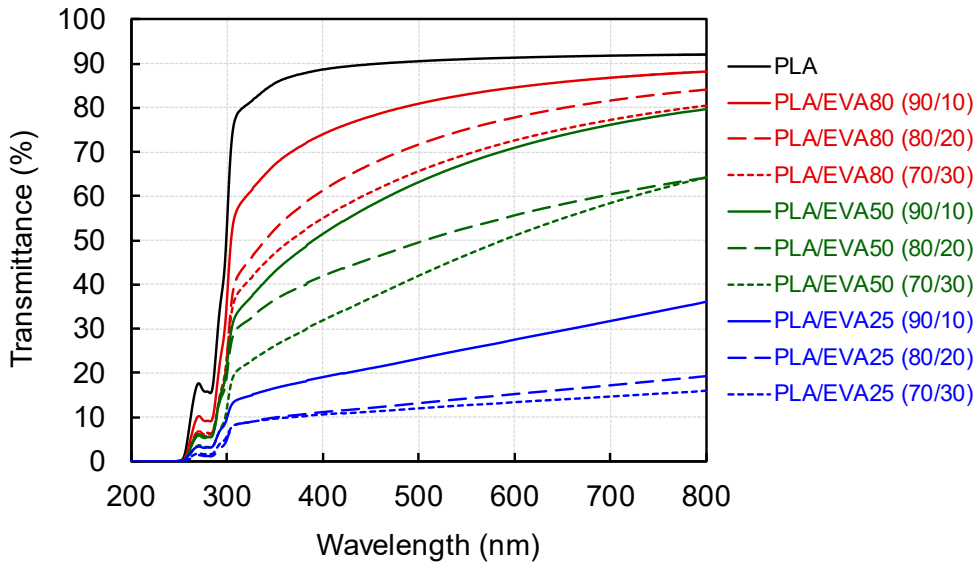

Figure 6 Wavelength dispersion of light transmittance.

Table 5 Haze values

Samples	PLA (wt.%)	EVA (wt.%)	*Haze* (%)
PLA	100	0	3
PLA/EVA25	90	10	86
	80	20	89
	70	30	90
PLA/EVA50	90	10	35
	80	20	59
	70	30	60
PLA/EVA80	90	10	14
	80	20	22
	70	30	29

Mechanical properties

The stress–strain curves at 25 °C are shown in Fig. 7. Both stress and strain are the engineering values. The pure PLA underwent brittle fracture when stretching commenced, which is a well-known behavior [1-4,11,12]. The yield points detected in

the blends suggest that the mechanical toughness was improved by the EVA addition to some degree, at least at the stretching speed applied in this study, that is, an initial strain rate of 0.35 s^{-1}. The elongation at break increased with the EVA content in the PLA/EVA80 blends, as summarized in Fig. 8, whereas it decreased with the EVA content in the PLA/EVA25 blends. The low values of elongation at break for PLA/EVA25 (80/20) and (70/30) may be attributed to the excess stress concentration at the interface due to the large size of dispersed EVA particles, which resulted in brittle fracture via crack/craze formation.

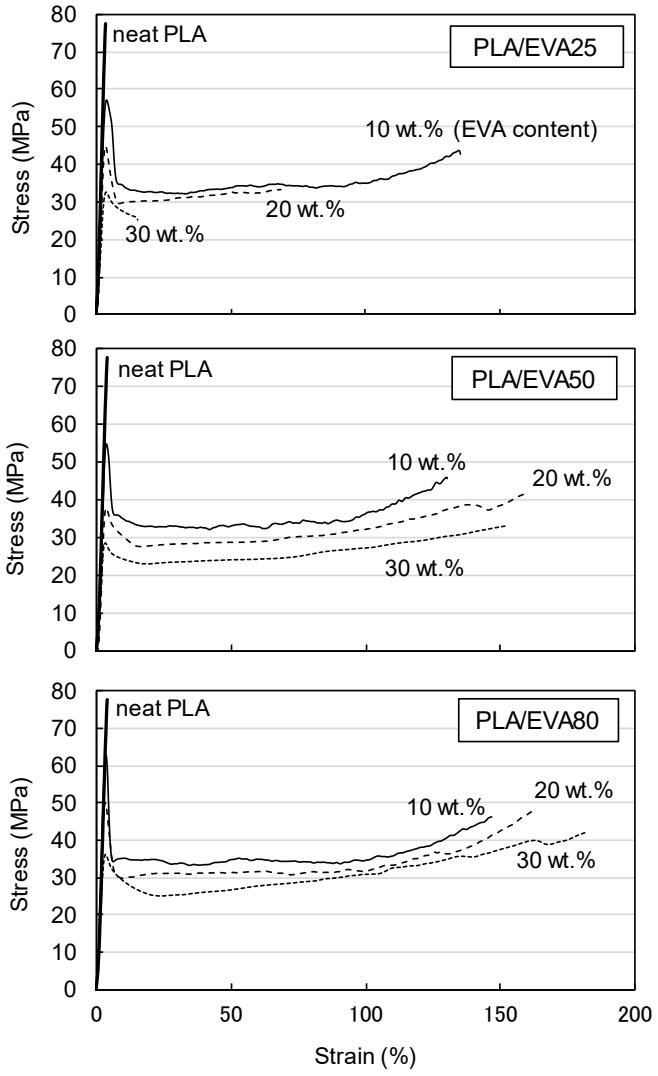

Figure 7 Stress-strain curves

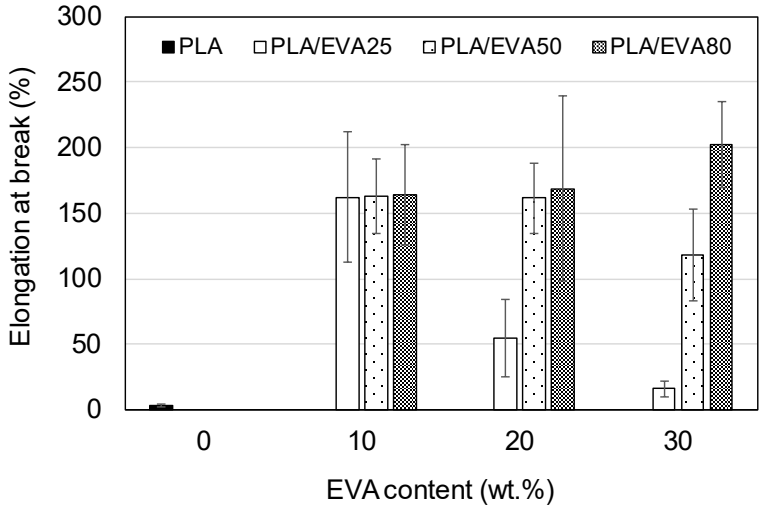

Figure 8 Elongation at break

The film impact strengths at 25 °C are summarized in Fig. 9. The addition of EVA25 slightly enhanced the impact strength. However, the strength decreased with increasing the EVA25 content. This may be attributed to the coarse morphology, as corroborated by the tensile test; i.e., a high stress concentrated at the interface is responsible for the crack/craze formation. In contrast, the impact strength was markedly improved by the addition of EVA50 or EVA80. Furthermore, the strength of the blends also increased with increasing the EVA content.

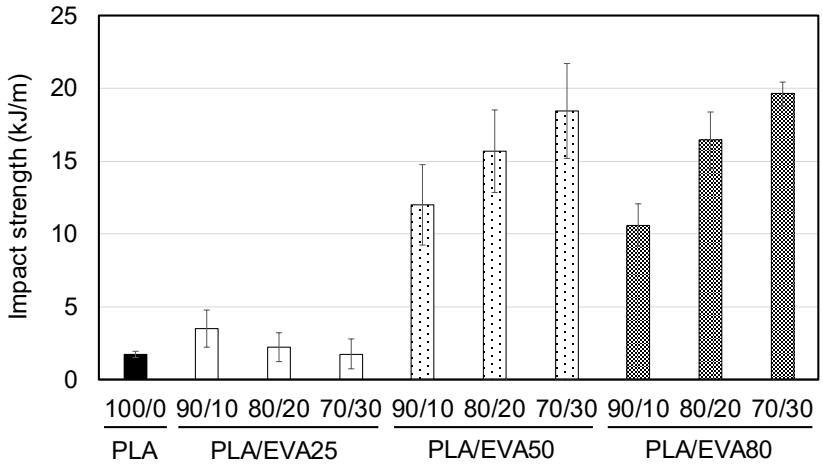

Figure 9 Film impact strength

Fig. 10 shows the appearance of the samples after the film impact tests. The samples with low impact strength—PLA and PLA/EVA25 (80/20)—exhibited brittle fractures with well-developed crack propagation. In contrast, we detected intense stress whitening in the samples with high impact strength, that is, the PLA/EVA50 and PLA/EVA80 blends. The stress whitening behavior is a key factor to understand the mechanical toughness [13-15,43-45]. Therefore, the morphology in the stress whitening region was investigated in detail by TEM.

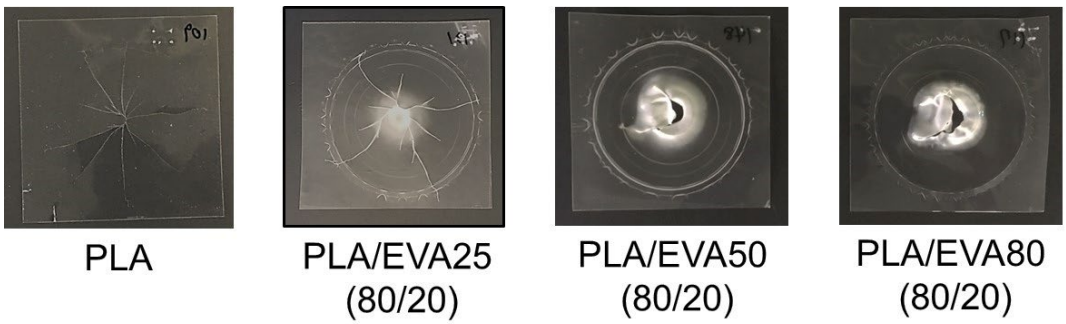

Figure 10 Appearance of the samples after the film impact tests.

Fig. 11 shows the TEM images after the impact tests. There was a marked difference in the formation of voids and cracks among the samples. In PLA/EVA25 (80/20), the cracks grew at the interface between the matrix and the droplets. This failure suggests the weak adhesion at the phase boundary due to high interfacial tension, i.e., thin interfacial thickness. Large dispersed particles with low interfacial strength result in poor mechanical toughness and crack propagation, which is presumably originated at the interface. In contrast, there was cavitation—void opening in the rubber

dispersion—in PLA/EVA80 (80/20). Cavitation, which must be the origin of the light scattering, reduces dilatational stress, providing ductility [43-45]. The differences in the fracture behavior between the samples must originate from the droplet size and the interfacial strength. The former is responsible for the stress concentration, and the latter affects the fracture point, that is, the interface between the phases or inside the dispersed particles. The interfacial strength is determined by the interfacial thickness due to the increase in the entanglement couplings. The interfacial thickness is known to be inversely proportional to the interfacial tension [34]. According to Wool, furthermore, the adhesive strength between immiscible polymers is proportional to the square root of interfacial thickness [46].

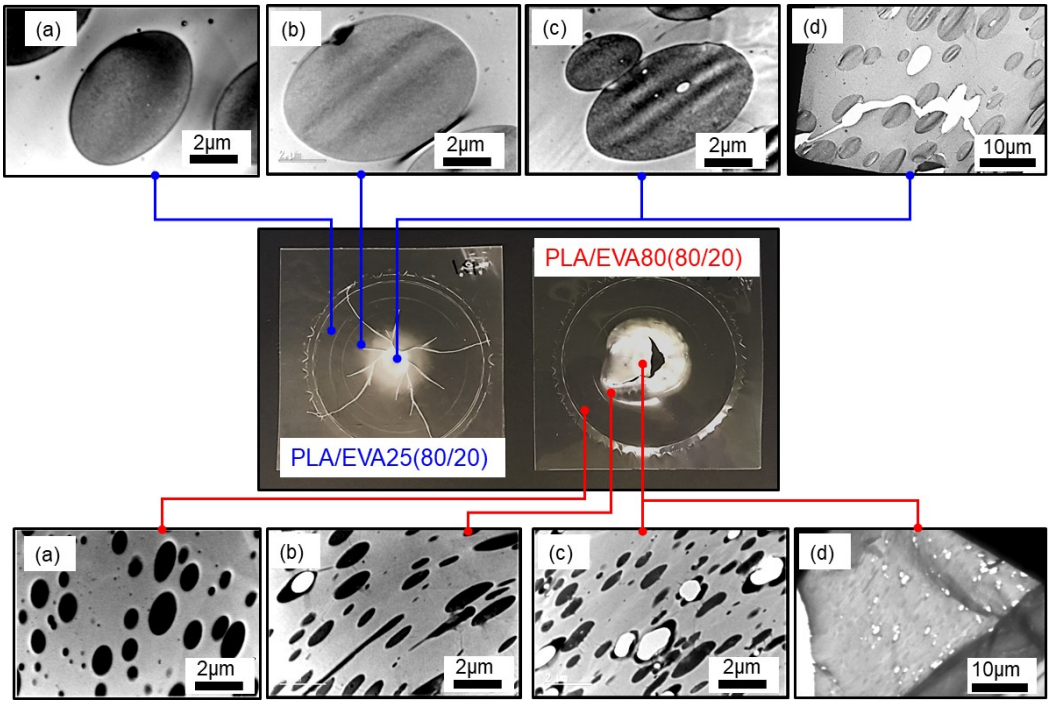

Figure 11 Morphologies of the samples after the impact tests. (top) PLA/EVA25 (80/20) and (bottom) PLA/EVA80 (80/20).

Fig. 11 reveals that there was no droplet deformation in PLA/EVA25 (80/20), although the dispersed droplets were markedly deformed in PLA/EVA80 (80/20). Considering that the sample films were prepared by compression molding with a long heating period, which relaxed the orientation/deformation of EVA droplets, as shown in Fig. 11(a), the prolonged droplets suggest that shear yielding occurred in the matrix in PLA/EVA80 (80/20). Shear yielding is dominant in immiscible polymer blends when the matrix ligament thickness is shorter that the critical value [47]. Fig. 12 illustrates the relationship between the matrix ligament thickness and the film impact strength in the PLA/EVA blends. The impact strength increased when the ligament thickness was below the critical value—approximately 2 μm—irrespective of the EVA content.

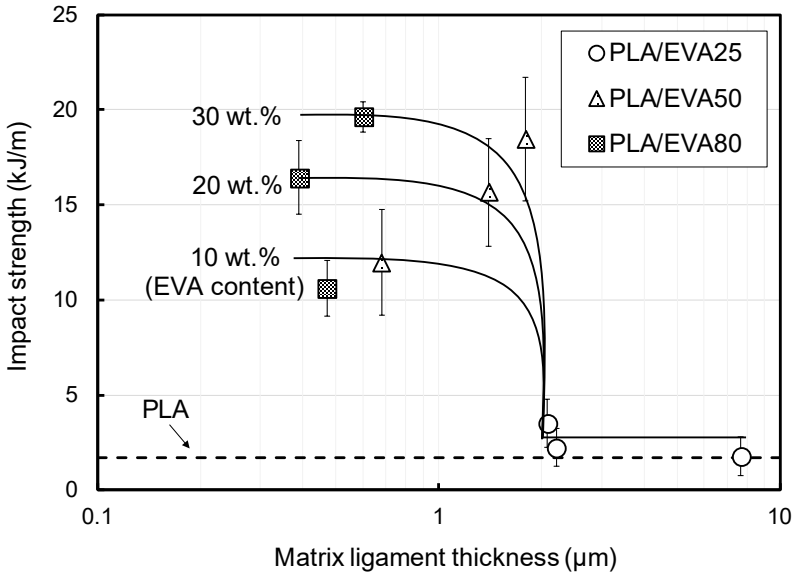

Figure 12 Relationship between matrix ligament thickness and impact strength

The experimental results demonstrate that cavitation in the dispersed droplets and massive shear yielding in the PLA matrix were responsible for the mechanical

performance. The addition of EVA containing a high VAc content provides both mechanisms, thereby improving the mechanical toughness of PLA.

Conclusions

We investigated the effects of the addition of EVA on the optical and mechanical properties for PLA using three EVA samples with various VAc contents. The VAc content in EVA had a critical effect on the structure and properties of the blends. The interfacial tension with PLA decreased with increasing VAc content. Therefore, the dispersed EVA droplets were small in the blends containing EVA with a high VAc content, that is, EVA50 and EVA80. The elongation at break and the film impact strength were greatly improved, especially by the addition of EVA50 and EVA80. The detailed characterization of the fractured areas after the impact tests indicates that both shear yielding and cavitation occurred in the blends, indicating enhanced mechanical toughness. In contrast, the EVA25 blends exhibited brittle fracture with well-developed crack propagation. This was due to the weak interfacial strength between EVA and PLA, and the presence of large dispersed droplets, which resulted in excess stress concentration. The VAc content in EVA also affected the light transmittance, because the difference in the refractive indices of the components decreased with increasing the VAc content. The small size of the dispersed particles also helped to reduce light scattering. In conclusion, the addition of EVA80 greatly improves the mechanical toughness of PLA without sacrificing its optical transparency.

References

[1] R. Auras, L.T. Lim, S.E.M. Selke, H. Tsuji, Poly(lactic acid): Synthesis, structures, properties, processing, and applications, Wiley, Hoboken, 2010.

[2] S. Saeidlou, M.A. Huneault, H.B. Li, C.B. Park, Poly(lactic acid) crystallization, Prog. Polym. Sci. 37 (2012) 1657-1677.

[3] A. Jimenez, M. Peltzer, R. Ruseckaite, Poly(lactic acid) science and technology: Processing, properties, additives, and applications, RSC Publishing, Oxfordshire, 2014.

[4] M. Yamaguchi, Manufacturing of high-performance biomass-based polyesters by rheological approach, in V.K. Thakur, M.K. Thakur, M.R. Kessler, (Eds.) Handbook of composites from renewable materials, Wiley, Hoboken, 2016, Chap.2.

[5] S.S. Ray, M. Bousmina, Biodegradable polymers and their layered silicate nanocomposites: In greening the 21st century materials world. Prog. Materials Sci. 50 (2005) 962-1079.

[6] T. Huang, M. Miura, S. Nobukawa, M. Yamaguchi, Crystallization behavior and dynamic mechanical properties of poly(L-lactic acid) with poly(ethylene glycol) terminated by benzoate, J. Polym. Environment 22 (2014) 183-189.

[7] H. Yamane, K. Sasai, M. Takano, and M. Takahashi, Poly(D-lactic acid) as a rheological modifier of poly(L-lactic acid): Shear and biaxial extensional flow behavior, J. Rheol. 48 (2004) 599-609.

[8] R. Dhavalikar, M. Yamaguchi, M. Xanthos, Molecular and structural analysis of a triepoxide-modified poly(ethylene terephthalate) from rheological data, J. Polym. Sci. Part A: Polym. Chem. 41 (2003) 958-969.

[9] T. Yokohara, S. Nobukawa, M. Yamaguchi, Rheological properties of polymer composites with flexible fine fiber, J. Rheol. 55 (2011) 1205-1218.

[10] M. Yamaguchi, T. Yokohara, B.M.A. Mohd Amran, Effect of flexible fibers on rheological properties of poly(lactic acid) composites under elongational flow, Nihon Reoroji Gakkaishi 41 (2013) 129-135.

[11] T. Huang, M. Miura, S. Nobukawa, M. Yamaguchi, Chain packing and its

anomalous effect on mechanical toughness for poly(lactic acid), Biomacromolecules 16 (2015) 1660-1666.

[12] T. Huang, M. Yamaguchi, Effect of cooling conditions on the mechanical properties of crystalline poly(lactic acid), J. Appl. Polym. Sci. 134 (2017) 44960-44966.

[13] H.H. Kausch, Polymer fracture, Springer-Verlag, Berlin, 1987.

[14] A.J. Kinloch, R.J. Young, Fracture behaviours of polymers, Springer, 1998.

[15] A.S. Argon, The physics of deformation and fracture of polymers, Cambridge University Press, New York, 2013.

[16] D. Wu, Y. Zhang, L. Yuan, M. Zhang, W. Zhou, Viscoelastic interfacial properties of compatibilized poly(ε-caprolactone)/polylactide blend, J. Polym. Sci. Part B, Polym. Phys. 48 (2010) 756–765

[17] M. Harada, T. Ohya, K. Iida, H. Hayashi, K. Hirano, H. Fukuda, Increased impact strength of biodegradable poly(lactic acid)/poly(butylene succinate) blend composites by using isocyanate as a reactive processing agent, J. Appl. Polym. Sci. 106 (2007) 1813–1820.

[18] T. Yokohara, M. Yamaguchi, Structure and properties for biomass-based polyester blends of PLA and PBS, Eur. Polym. J. 44 (2008) 677–685.

[19] L. Jiang, M.P. Wolcott, J. Zhang, Study of biodegradable polylactide/poly(butylene adipate-co-terephthalate) blends, Biomacromolecules 7 (2006) 199-207.

[20] J.J. Han, H.X. Huang, Preparation and characterization of biodegradable polylactide/thermoplastic polyurethane elastomer blends, J. Appl. Polym. Sci. 120 (2011) 3217-3223.

[21] T. Li, L.S. Turng, Polylactide, nanoclay, and core–shell rubber composites, Polym. Eng. Sci. 46 (2006) 1419-1427.

[22] N. Zhang, Q. Wang, J. Ren, L. Wang, Preparation and properties of biodegradable poly(lactic acid)/poly(butylene adipate-co-terephthalate) blend with glycidyl methacrylate as reactive processing agent, J. Mater. Sci. 44 (2009) 250-256.

[23] Y. Li, H. Shimizu, Improvement in toughness of poly(L-lactide) (PLLA) through reactive blending with acrylonitrile-butadiene-styrene copolymer (ABS):

Morphology and properties, Eur. Polym. J. 45 (2009) 738-746.

[24] K.S. Anderson, S.H. Lim, M.A. Hillmyer, Toughening of polylactide by melt blending with linear low-density polyethylene, J. Appl. Polym. Sci. 89 (2003) 3757-3768.

[25] A.M. Gajria, V. Dave, R.A. Gross, S.P. McCarthy, Miscibility and biodegradability of blends of poly(lactic acid) and poly(vinyl acetate), Polymer, 37 (1996) 437–444.

[26] P. Ma, D.G.H. Bogaerds, J.G.P. Goossens, A.B. Spoelstra, Y. Zhang, P.J. Lemstra, Toughening of poly(lactic acid) by ethylene-co-vinyl acetate copolymer with different vinyl acetate contents, Eur. Polym. J. 48 (2012) 146-154.

[27] R.K. Singla, M.T. Zafar, S.N. Maiti, A.K. Ghosh, Physical blends of PLA with high vinyl acetate containing EVA and their rheological, thermo-mechanical and morphological responses, Polym. Testing 63 (2017) 398-406.

[28] R.K. Singla, S.N. Maiti, A.K. Ghosha, Fabrication of super tough poly(lactic acid)/ethylene-*co*-vinyl-acetate blends via a melt recirculation approach: static-short term mechanical and morphological interpretation, Roy. Soc. Chem. 6 (2016) 14580-14588.

[29] P.A. Small, Some factors affecting the solubility of polymers, J. Appl. Chem. 3 (1953) 71-80

[30] H.E.H. Meijer, J.M.H. Janssen, P.D. Anderson, Mixing of immiscible liquids, in I. Manas-Zloczower (Ed.) Mixing and compounding of polymers, 2nd ed., Hanser: Munich, 2009, Chap. 3.

[31] M. Yamaguchi, S. Abe, LLDPE/LDPE blends. Part 1. Rheological, thermal, and mechanical properties, J. Appl. Polym. Sci. 74 (1999) 3153-3159.

[32] S. Takahashi, H. Okada, S. Nobukawa, M. Yamaguchi, Optical properties of polymer blends composed of poly(methyl methacrylate) and ethylene–vinyl acetate copolymer, Eur. Polym. J. 48 (2012) 974-980.

[33] D.K. Owens, R.C. Wendt, Estimation of the surface free energy of polymers, J. Appl. Polym. Sci. 13 (1969) 1741-1747.

[34] M. Yamaguchi, Effect of molecular structure in branched polyethylene on adhesion properties with polypropylene, J. Appl. Polym. Sci. 70 (1998) 457-463.

[35] R. Wiwattananukul, B. Fan, M. Yamaguchi, Improvement of rigidity for rubber-toughened polypropylene via localization of carbon nanotubes, Comp. Sci. Technol. 141 (2017) 106-112.

[36] Y. Zhang, S. Park, In situ shear-induced mercapto group-activated graphite nanoplatelets for fabricating mechanically strong and thermally conductive elastomer composites for thermal management applications, Comp. Part A: Appl. Sci. Manuf. 112 (2018) 40-48.

[37] Y. Zhang, U.R. Cho, Enhanced thermo-physical properties of nitrile-butadiene rubber nanocomposites filled with simultaneously reduced and functionalized graphene oxide, Polym. Comp. 39 (2018) 3227-3235.

[38] Y. Zhang, J.R. Choi, S. Park, Enhancing the heat and load transfer efficiency by optimizing the interface of hexagonal boron nitride/elastomer nanocomposites for thermal management applications, Polymer 143 (2018) 1-9.

[39] S. Wu, Formation of dispersed phase in incompatible polymer blends: Interfacial and rheological effects, Polym. Eng. Sci. 27 (1987) 335-347.

[40] Z.H. Liu, X.D. Zhang, X.G. Zhu, Z.N. Qi, F.S. Wang, Effect of morphology on the brittle ductile transition of polymer blends: 1. A new equation for correlating morphological parameters, Polymer 38 (1997) 5267-5273.

[41] H. Shimada, A. Kiyama, P. Phulkerd, M. Yamaguchi, Anomalous optical anisotropy of oriented cellulose triacetate film, Nihon Reoroji Gakkaishi 45 (2017) 19-24.

[42] R. Osato, T. Sako, J. Seemork, S. Arayachukiat, S. Nobukawa, M. Yamaguchi, Self-healing properties of poly(ethylene-co-vinyl acetate), Colloid Polym. Sci. 294 (2016) 537-543.

[43] M. Yamaguchi, K. Nitta, Optical and acoustic investigation of binary blends of polypropylene with ethylene-α-olefin copolymer, Polym. Eng. Sci. 39 (1999) 833-840.

[44] R.J. Gaymans, Toughening of semicrystalline thermoplastics, in D.R. Paul, C.B. Bucknall (Eds.), Polymer blends, Wiley, New York, 2000, Chap. 25.

[45] M. Yamaguchi, Mechanical properties and structure of rubber-toughened immiscible blends, in S. Kobayashi, K. Müllen (Eds.), Encyclopedia of polymeric nanomaterials, Springer-Verlag, Berlin, 2015, pp.1214-1218.

[46] R.P. Wool, Polymer interfaces: Structure and strength. Hanser Gardener, Cincinnati, 1994.

[47] S. Wu, Chain structure, phase morphology, and toughness relationships in polymers and blends, Polym. Eng. Sci. 30 (1990) 753-801.